ChemPhysChem

Research Article
doi.org/10.1002/cphc.202500680

Chemistry Europe
European Chemical Societies Publishing

www.chemphyschem.org

Refractive Indices and Infrared Band Strengths of Amorphous Ices of Key Fluorinated Refrigerants 1,1,1,2-Tetrafluoroethane, 2,3,3,3-Tetrafluoropropene, and 3,3,3-Trifluoropropene

Koushik Mondal, Mason McAnally, Souvick Biswas, Nils W. Melbourne, Andrew M. Turner, Alexandre Bergantini, Rui Sun,* and Ralf I. Kaiser*

Hydrofluorocarbons (HFCs), a class of polyfluorocarbon (PFC), represent a key group of chemicals exploited extensively in refrigeration and innovative future technological cooling applications. To separate, purify, and reuse HFCs, spectroscopic properties of these compounds must be available. To quantify these materials under cryogenic conditions, a condensed-phase spectroscopic investigation of their physical parameters is required. Herein, the optical and spectroscopic properties of HFCs used as refrigerant at low temperature (10 K) are investigated. Refractive indices of 1,1,1,2-tetrafluoroethane (CF_3CH_2F; HFC134a), 2,3,3,3-tetrafluoropropene ($CF_3CF{=}CH_2$; R1234yf), and 3,3,3-trifluoropropene ($CF_3CH{=}CH_2$; R1243zf) are found to be 1.24 ± 0.02, 1.34 ± 0.02, and 1.30 ± 0.02, respectively. Infrared band strengths of the abovementioned HFC ices on a cold silver substrate are measured utilizing absorption reflection infrared spectroscopy. The fundamental vibrational modes are analyzed using quantum chemical calculations in tandem with vibrational spectroscopic analysis. The strongest infrared absorption corresponds to combined C—F vibrational modes originating from CF_3 group and olefinic C—F bonds, which has band strengths ranging 2×10^{-18} to 3×10^{-18} cm molecule^{-1}. Comparisons of solid and vapor-phase spectra show vibrational shifts, aiding understanding of solid-state interactions and ice formation. These findings enhance knowledge of low-temperature HFC chemistry, focusing on optical and spectroscopic changes during ice development.

1. Introduction

Perfluorocarbons (PFCs) are a class of chemical compounds distinguished by their exceptional stability, nonflammability, low surface tension, and minimal solubility. These properties render them highly valuable across a broad array of applications, ranging from household products to industrial processes. Notably, a significant subset of fluorinated gases, particularly hydrofluorocarbons (HFCs), is extensively produced and utilized in refrigeration and air conditioning systems.[1–3] Moreover, HFCs are being explored for innovative technological applications, including liquid thin film technologies in aviation and aerospace sectors, as well as advanced cooling systems employing supersonic jet nozzles.[4–6] Ongoing research aims to develop future cooling technologies tailored for critical sectors, emphasizing efficiency and environmental safety.

Despite their widespread use, the environmental fate of HFCs remains not completely understood from a molecular perspective. Specifically, the mechanisms underlying their photolytic breakdown and oxidation are not fully elucidated, particularly in the context of upper tropospheric conditions and low-temperature cloud formation.[7–10] This knowledge gap raises concerns about the potential long-term atmospheric consequences of HFC emissions. Consequently, regulatory measures are in place, and researchers are actively exploring policies that promote the recycling of legacy refrigerants, the adoption of environmentally benign alternatives, and the reduction of unintentional atmospheric emissions.[8,11,12]

Recycling methods for refrigerants, such as cryogenic separation techniques, membrane-assisted cryogenic separation,[13–15] and extractive distillation using ionic liquids,[16–18] are considered highly effective. These techniques are especially crucial for managing environmentally hazardous HFCs used in ultralow temperature refrigeration systems, which operate between 223 K and 123 K.[19] Such systems are vital for pharmaceutical and biological applications, where current alternatives are limited. Implementing these advanced recycling methods can significantly reduce environmental risks associated with the disposal and reuse of refrigerants in sensitive applications. New generation refrigerants like 2,3,3,3-tetrafluoropropene (R-1234yf) are already replacing older compounds such as

K. Mondal, M. McAnally, S. Biswas, N. W. Melbourne, A. M. Turner, A. Bergantini, R. Sun, R. I. Kaiser
Department of Chemistry
University of Hawai'i at Manoa
Honolulu, Hawaii 96822, USA
E-mail: ruisun@hawaii.edu
ralfk@hawaii.edu

A. Bergantini
Valongo Observatory
Federal University of Rio de Janeiro (OV-UFRJ)
Rio de Janeiro, RJ 20080-090, Brazil

Supporting information for this article is available on the WWW under https://doi.org/10.1002/cphc.202500680

1,1,1,2-tetrafluoroethane (HFC-134a) in household and automotive industries,[10,20–23] but substantial gaps remain in understanding their environmental behavior, especially under tropospheric conditions. Concerns have been raised about the formation of persistent chemicals like trifluoroacetic acid (CF_3COOH) during their breakdown, which could have significant impacts on the atmospheric chemistry, particularly in low-temperature environments.[24–26] Recent advancements in optical spectroscopic techniques have facilitated the investigation of these processes at the molecular level, providing insights into their behavior in the upper troposphere.[27,28]

Progress in utilizing the unique properties of HFCs for technological applications, combined with the development of cryogenic separation techniques and studies of low-temperature interactions, underscores the need for reliable spectroscopic quantification of refrigerants under such conditions.[18,29–31] Although infrared and Raman spectroscopy have been employed to study refrigerants in gas and liquid phases, comprehensive vibrational assignments related to molecular interactions, and the quantification of key optical and spectroscopic parameters such as refractive index, band strength in solid amorphous ices, remain limited.[32–40] Addressing these gaps is essential for advancing our understanding of refrigerant behavior in cold environments.

This combined experimental and computational study aims to quantify critical optical and spectroscopic parameters, including refractive index and infrared band strength. Fundamental spectroscopic properties were determined by exploiting laser interferometry and absorption reflection Fourier transform infrared spectroscopy (FTIR) from the vapor deposited ices of the refrigerants at low-temperature. Such data that are essential to understand their upper tropospheric chemistry. The first system of interest in this aspect is the most extensively used refrigerant for the last several decades, HFC134a [1,1,1,2-tetrafluoroethane; CF_3CH_2F; (R-I)]. Additionally, the study investigates newer hydrofluoroolefins (HFOs), such as R-1234yf [2,3,3,3-tetrafluoropropene; $CF_3CF{=}CH_2$; (R-II)] and R-1243zf [3,3,3-trifluoropropene; $CF_3CH{=}CH_2$; (R-III)], which are gaining prominence as environmentally friendlier alternatives (**Table 1**). Overall, this research opens a new and largely unexplored avenue for understanding the low-temperature quantification of HFCs and the evolution of distinctive spectral features in the solid state, further supporting the development of sustainable cooling technologies that minimize ecological impact.

2. Experimental and Computational Section

A schematic presentation of the experimental arrangement is shown in **Figure 1**. Briefly the experiments were conducted in an ultrahigh vacuum chamber manufactured from low-carbon stainless steel type 304.[41–45] The chamber was evacuated to a base pressure of 5×10^{-11} torr using an oil-free, magnetically levitated turbomolecular pump (Osaka, Pump Model TG1121 MCA) in series with a second turbomolecular pump (Osaka, Pump Model TG420 MCAC) backed by an oil-free scroll pump (Edwards, XDS35i). At the center of the chamber, a silver substrate serves as the target affixed to a cold head (CTI Cryodyne 1020C); this target was cooled to 10 ± 0.5 K by a two-stage closed-cycle helium refrigerator (Cryodyne 9600 compressor). The cold head was connected to a differentially pumped rotatable flange allowing the silver target to rotate freely within the experimental plane. The gas deposition onto the target was done by introducing each gas in separate experiments through a glass capillary array with 10 μm pores controlled by a precision leak valve (Figure 1). Neat refrigerant ices were prepared by depositing 99.9% 1,1,1,2-tetrafluoroethane (R-I) (Chemours), 2,3,3,3-tetrafluoropropene (R-II) (Chemours), and 3,3,3 trifluoropropene (R-III) (Pfaltz & Bauer) at pressures of some 5×10^{-7} torr. The growth patterns of the ice films were controlled by the deposition time and monitored in situ via laser interferometry (Section 2.1).

2.1. Laser Interferometry

Laser interferometry is primarily used for determining refractive indices, band strengths, and thicknesses of vapor-deposited ices.[41–47] A helium-neon (HeNe) laser with an output of 632.8 nm (λ) (Melles Griot 25-LHP-213, 0.5 mW) is reflected off the silver substrate during the deposition at an angle specified in Figure 1b. The power of the reflected light was monitored with a calibrated photodiode (Thorlabs SM1PD1A) connected to a picoammeter (Keithley 6485) and recorded versus the time using a LabVIEW script. The interference patterns resulting from the constructive and destructive interference between the portion of the laser that reflects off the ice surface and the portion that transmits through the ice and reflects off the silver substrate (Figure 1b) as the ice layer grows, thus altering the optical path difference and phase. Two lasers were positioned at different angles relative to the perpendicular plane of

Table 1. Compilation of molecular structures, formulae, common names, and abbreviations used in this publication.

Structure	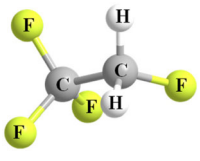	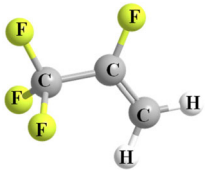	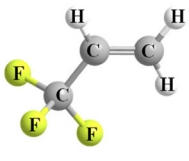
Molecular formula	CF_3CH_2F	CF_3CFCH_2	CF_3CHCH_2
IUPAC name	1,1,1,2-tetrafluoroethane	2,3,3,3-tetrafluoropropene	3,3,3-trifluoropropene
Common name	HFC134a	R-1234yf	R-1243zf
Name used here	R-I	R-II	R-III

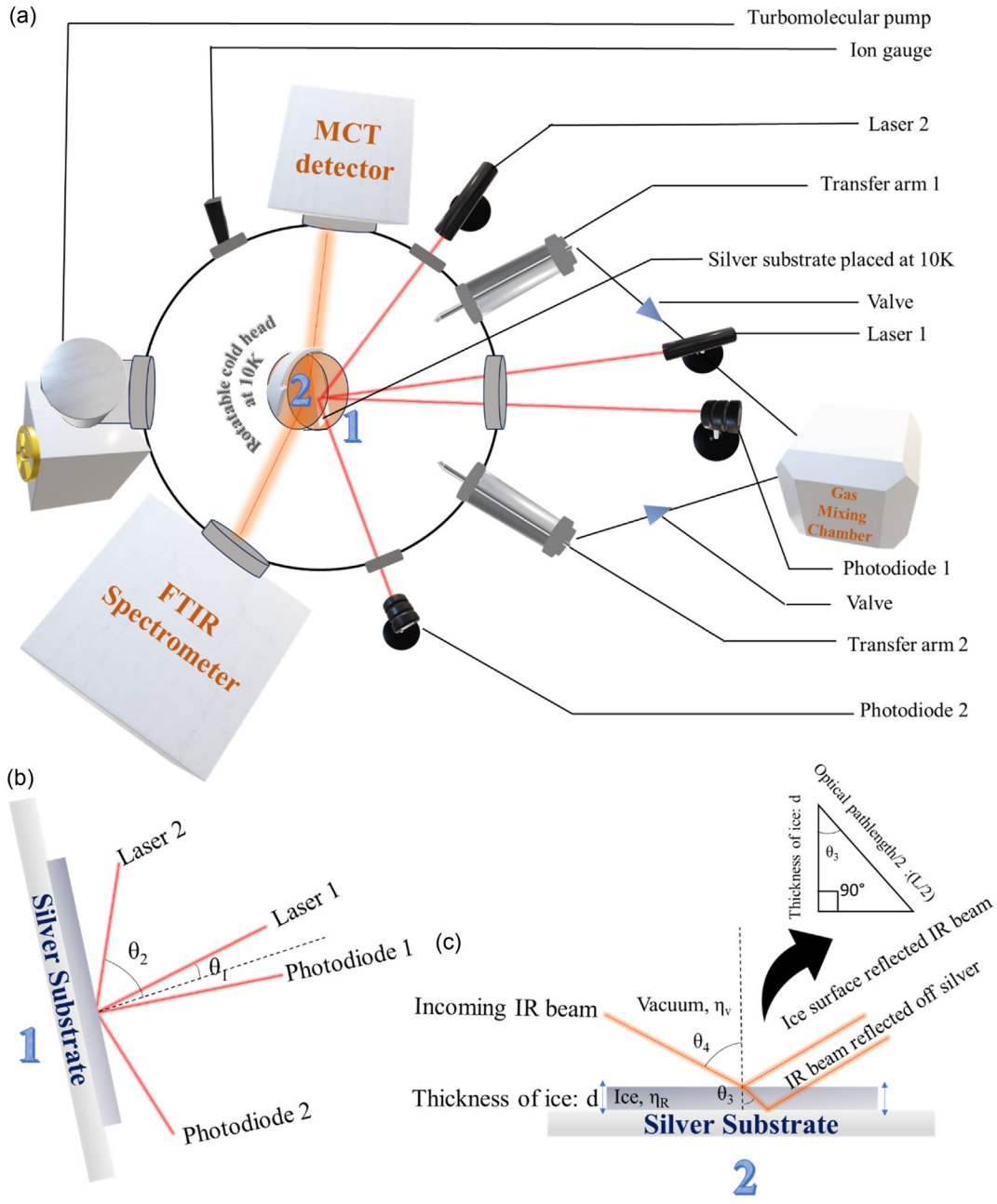

Figure 1. Schematic representation of the a) experimental setup, b) laser interferometry setup, and c) beam path.

the silver substrate—Laser 1 at (1.9° ± 0.1°) (θ_1) and Laser 2 at (54.8° ± 0.1°) (θ_2)—through conflat (CF) interfaced quartz windows as shown in Figure 1b. The periods between two fringes in the interference patterns for two lasers (T_1 and T_2) are utilized to calculate refractive index (η_R) according to Equation (1).[41]

$$\eta_R^2 = \frac{\frac{T_2^2}{T_1^2}\sin^2\theta_2 - \sin^2\theta_1}{\frac{T_2^2}{T_1^2} - 1} \quad (1)$$

The calculated refractive index (η_R) is further utilized to determine ice thickness (d) via same laser interferometry scheme by determining the fringes (n), where λ is the wavelength of the HeNe laser (632.8 nm). This ice thickness (d) combined with an infrared spectrum is necessary to determine infrared band strengths (Section 2.2.).

$$d = \frac{n\lambda}{2\sqrt{\eta_R^2 - \sin^2\theta_1}} \quad (2)$$

Although different thickness ices can be prepared exploiting laser interferometry, there exists some limitations related to ice thickness depending on refractive index, wavelength of the laser used, as well as number of fringes formed during deposition.

2.2. Spectroscopic Measurement

To collect infrared spectra at various thicknesses, amorphous ices of specific thicknesses were deposited by introducing refrigerant vapors onto a cold silver substrate at position 1, followed by rotating the substrate to position 2 to record the FTIR spectra in absorption–reflection mode at a 75° reflection angle with respect to the perpendicular axis of silver substrate (Figure 1c). FTIR spectroscopy in the range of 500 cm^{-1} to 5000 cm^{-1} was used to measure the infrared band strength. The Nicolet 6700 FTIR spectrometer (Thermo Scientific), equipped with customized external copper mirror optics, has been operated in absorption–reflection mode at a 75° reflection angle (Figure 1c, θ_3). The IR beam was focused on the silver substrate through a 35 mm zinc-selenide (ZnSe) window mounted on a CF flange. The reflected IR beam exits through a similar window, was recollimated, and directed to a liquid nitrogen-cooled mercury cadmium telluride (MCT-B) detector via second-stage transfer optics. Spectra were recorded over 30 min with a spectral resolution of 4 cm^{-1}, averaging 3360 scans per spectrum for improved signal-to-noise ratio. The infrared beam refracted within the ice at an angle θ_4, which is related to angle of incidence IR beam (θ_3) according to Snell's law as

$$\theta_4 = \sin^{-1}\frac{\eta_v}{\eta_R}\sin\theta_3 \tag{3}$$

Using this refraction angle optical path length (L), the IR beam that passes through a definite thickness (d) of ice can be determined as

$$L = \frac{2d}{\cos\theta_4} \tag{4}$$

Although the major objective of the study is to explore quantitative spectroscopic parameters like band strength, FTIR spectra of the deposited ices were also collected at various temperatures up to their sublimation from the silver substrate to gain additional spectroscopic insights.

Apart from the FTIR measurement of the vapor-deposited ice, gas-phase infrared spectra of each of the refrigerants were also recorded to compare the spectral shifts and intensity pattern at different stages. However, in this case, infrared spectra of the gases diluted in nitrogen (1:760) at a total pressure of 760 torr were recorded at a spectral resolution of 1 cm^{-1} in normal absorption mode.

2.3. Computational Methods

The geometries of the refrigerants were optimized, and infrared (IR) frequencies for 1,1,1,2-tetrafluoroethane (R-I), 2,3,3,3-tetrafluoropropene (R-II), and 3,3,3-trifluoropropene (R-III) were calculated with the NWChem program suite using density-functional theory at the B3LYP-D3/def2-TZVP level at 0 K.[48] The hybrid B3LYP functional offers a well-documented balance between accuracy and cost for vibrational spectroscopy of halogenated hydrocarbons, while the D3 dispersion correction is included to recover long-range interactions neglected by B3LYP.[49] The triple-zeta valence plus polarization def2-TZVP basis set provides near-basis-set-limit force constants for first-row and fluorine-substituted systems.[50] After full geometry optimization, analytic second derivatives were used to obtain harmonic vibrational wavenumbers. Unlike the usual harmonic frequency uniformly scaling as recommended by the NIST Computational Chemistry Comparison and Benchmark Database (CCCBD) for B3LYP/def2-TZVP experimental frequencies to compensate for systematic overestimation arising from the harmonic approximation and residual basis-set/functional deficiencies,[51] we calculated a calibration factor from the slope of the linear fit between experimentally measured frequencies at 10 K and theoretical frequencies at 0 K (Figure S1a–c, Supporting Information). The factor determined to be 0.983 ± 0.001, 1.004 ± 0.001, and 0.981 ± 0.001 for R-I, R-II, and R-III refrigerants, respectively.

3. Results and Discussions

3.1. Refractive Indices

The interference patterns of vapor-deposited refrigerant ices at 10 K are illustrated in **Figure 2**a–c for R-I, R-II, and R-III, respectively. For each refrigerant, the interference patterns obtained with the progress of deposition from the two lasers placed at distinct angles with respect to the perpendicular axis on silver substrate were distinctly different. The upper trace of each figure represents the interference pattern obtained for the photodiode current from the laser placed at $54.8° \pm 0.1°$ (θ_2) while lower trace represents interference pattern generated by the laser placed at an angle of $1.9° \pm 0.1°$ (θ_1) with respect to the perpendicular axis on silver substrate. It is important to note that these fringes should ideally be perfectly sinusoidal. However, fluctuations arising from laser stability and photodiode response can cause deviations in the resultant photodiode current from ideality. To accurately determine the periods T_1 and T_2 between consecutive fringes, the experimental data, defined by black traces, are smoothed (red) and fitted (green) using a modified sinusoidal function that accounts for these deviations, ensuring that the time axis aligns accurately. The modified sinusoidal function incorporates a linear decay component alongside the standard sine function, as described by Equation (5), which is necessary as reflectivity of the silver substrate decreases with the extent of ice deposition, resulting in decrease in overall photodiode current.

$$y = y_0 + A\sin\left(\pi\frac{x - x_c}{\omega}\right) + mx \tag{5}$$

where x_c represents the phase shift, ω is the period, A is the amplitude, y_0 is the initial offset, and m denotes the slope of the linear decay. The average time periods between consecutive fringes, derived from the fitted profiles, are taken as the actual periods $T_{n(1or2)}$. The phase shift error is considered as the measurement uncertainty in these periods. In **Table 2**, we summarize the fitted interference periods ($T_{n(1or2)}$) and the corresponding refractive indices (η_n) of three refrigerants, calculated using Equation (1). Our measured refractive index of a known, well-characterized amorphous

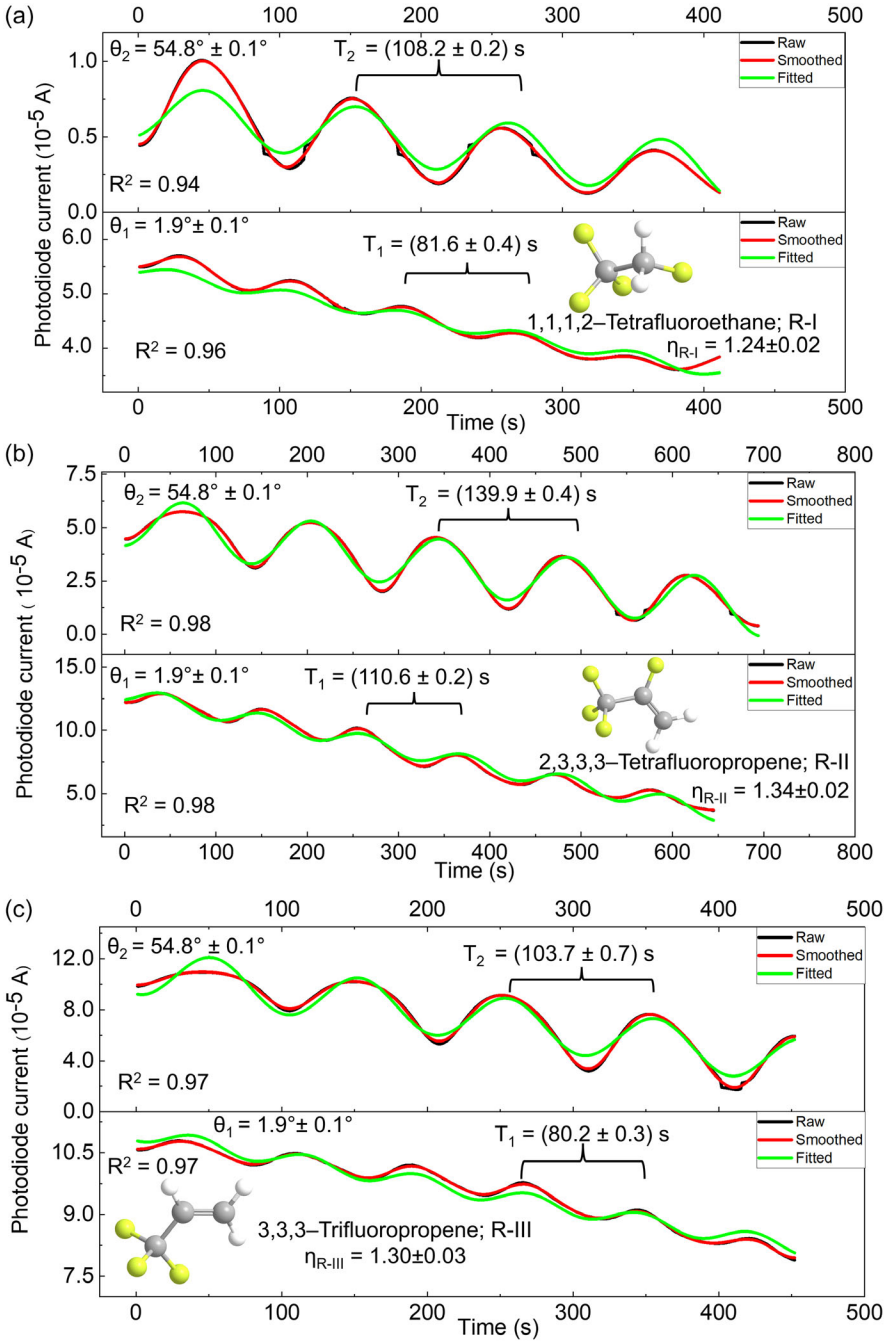

Figure 2. Interference patterns formed simultaneously during deposition at different angles in the two-laser interferometry setup. a) 1,1,1,2-Tetrafluoroethane (R-I), b) 2,3,3,3-tetrafluoropropene (R-II), c) 3,3,3-trifluoropropene (R-III).

methane ice at 10 K is compared with the reported literature value;[52] the fringe patterns are shown in Figure S2, Supporting Information. The measured refractive index of the amorphous methane ice of 1.36 ± 0.01 in our experiments closely aligns with the reported value of 1.34 ± 0.04. The experimentally measured refractive indices (η_n) of three refrigerants determined through this analysis at 10 K are 1.24 ± 0.02, 1.34 ± 0.02, and 1.30 ± 0.02 for R-I, R-II, and R-III, respectively. These refractive indices are crucial toward quantifying the integrated absorption coefficients, discussed later in the paper.[46]

3.2. Spectral Assignments and Infrared Band Strengths of Refrigerants in Amorphous Ices

Although the vibrational modes of HFCs are well established in the gas and liquid phases, quantitative information on their absorption coefficients in the solid phase is still insufficient. Previous spectroscopic studies of low-temperature solid HFCs have been mostly performed at 150 K, and quantitative information of the band strengths are lacking. The present, low-temperature, contamination-free, vapor deposition,

Table 2. Parameters obtained from the fitted interference profiles and corresponding refractive indices.

Name	Time period for laser-1 (T_1) [s]	Time period for laser-2 (T_2) [s]	Refractive index (η)
Methane	61.7 ± 0.3	76.9 ± 0.3	1.36 ± 0.02
1,1,1,2-tetrafluoroethane (R-I)	81.6 ± 0.4	108.2 ± 0.2	1.24 ± 0.02
2,3,3,3-tetrafluoropropene (R-II)	110.6 ± 0.2	139.9 ± 0.4	1.34 ± 0.02
3,3,3-trifluoropropene (R-III)	80.2 ± 0.3	103.7 ± 0.7	1.30 ± 0.03

combined with optical interferometry and highly sensitive absorption-reflection-absorption infrared spectroscopy, has the capability to meticulously monitor spectroscopic properties of thin ice layers down to a few nanometers with high accuracy. Additionally, we discuss spectral changes with varying ice layer thicknesses.

3.2.1. Band Assignments

For each of the refrigerant, infrared spectra corresponding to three different ice thicknesses (d) were recorded (**Figure 3–5**). The thicknesses of the ices were obtained via the number of fringes collected by laser interferometry similar to refractive index

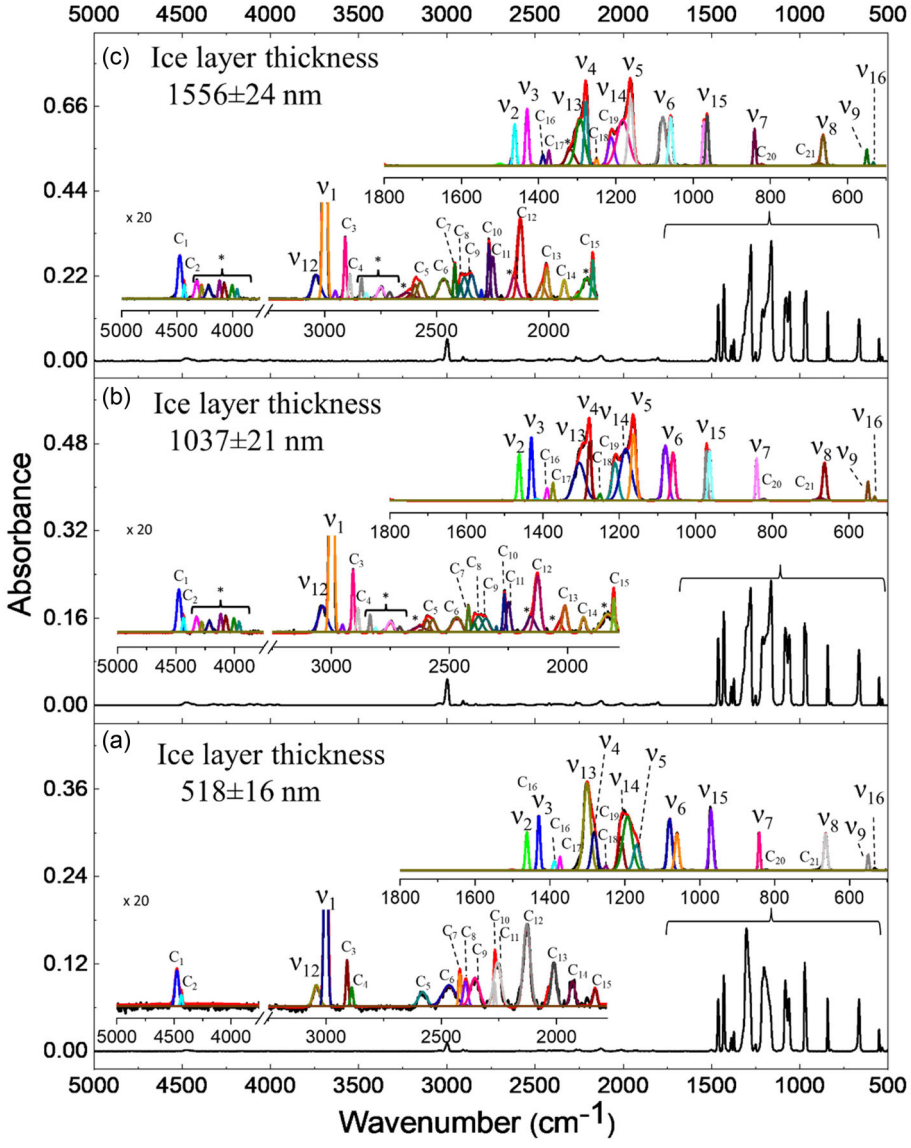

Figure 3. Infrared spectra of 1,1,1,2-tetrafluoroethane (R-I) at different ice thicknesses of a) 518 ± 16 nm, b) 1037 ± 21 nm, and c) 1556 ± 24 nm.

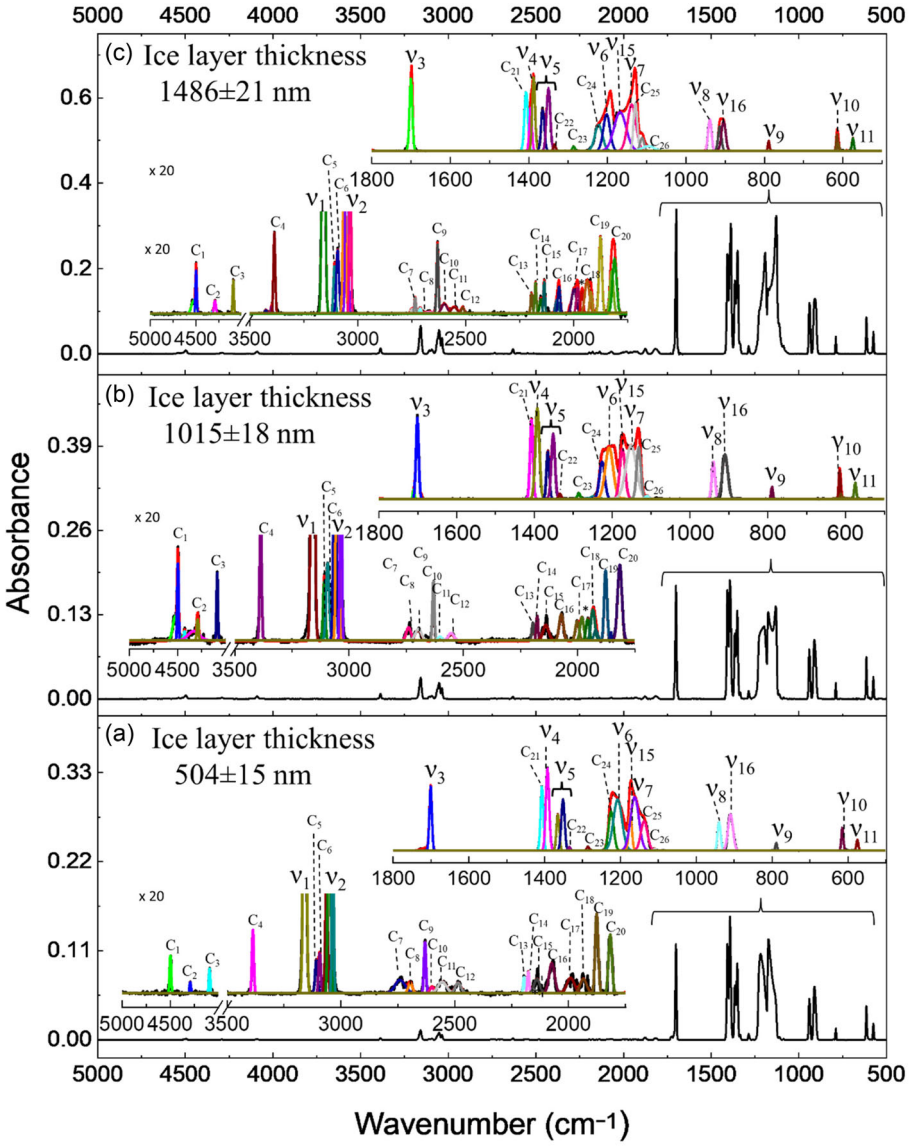

Figure 4. Infrared spectra of 2,3,3,3-tetrafluoropropene (R-II) at different ice thicknesses of a) 504 ± 15 nm, b) 1015 ± 18 nm, and c) 1486 ± 21 nm.

measurements. In case of R-I, the depositions of the refrigerant vapor on cold silver substrate were stopped after forming 2.0 ± 0.1, 4.1 ± 0.1, and 6.1 ± 0.1 fringes (*n*), whereas for R-II and R-III the number of fringes obtained were 2.1 ± 0.1, 4.3 ± 0.1, 6.3 ± 0.1 and 2.0 ± 0.1, 4.3 ± 0.1, and 6.2 ± 0.1, respectively, as shown in Figure S3a–c, Supporting Information. The corresponding thicknesses of the ices were calculated using Equation (2) (**Table 3**). The spectra revealed significant absorptions in the 500 cm^{-1} to 1500 cm^{-1} range due to fundamental bands along with a number of combination bands and overtones. To accurately assign fundamental bands at 10 K, we employed electronic structure theory calculations of the molecules and summarized in **Table 4–6**. The combination and overtone modes of each refrigerant are summarized in **Table 7–9**. New vibrational bands (asterisked) emerge for thicker ices as revealed via spectral deconvolution (Figure 3–5); (Table S1a–c, Supporting Information). The reliability of the computational method is benchmarked by comparing the calculated frequencies with the experimental ones as shown in Figure S1a–c, Supporting Information; calibration factors are calculated to be 0.983 ± 0.001, 1.004 ± 0.001, and 0.981 ± 0.001 for R-I, R-II, and R-III, respectively. A summary of the previously reported spectral bands in the gas, liquid, and solid phases is also provided for comparison of the solid-phase spectral frequency with literature assignments. The coordinates of the optimized structures of the refrigerants are provided in Table S2a–c, Supporting Information, while calculated fundamental frequencies are compiled Table 4–6.

The most prominent vibrational features are observed between 1000 cm^{-1} and 1400 cm^{-1}, mainly involving C—F vibrations. As there exists a significant number of vibrational modes, we are limiting our discussion to the five most intense

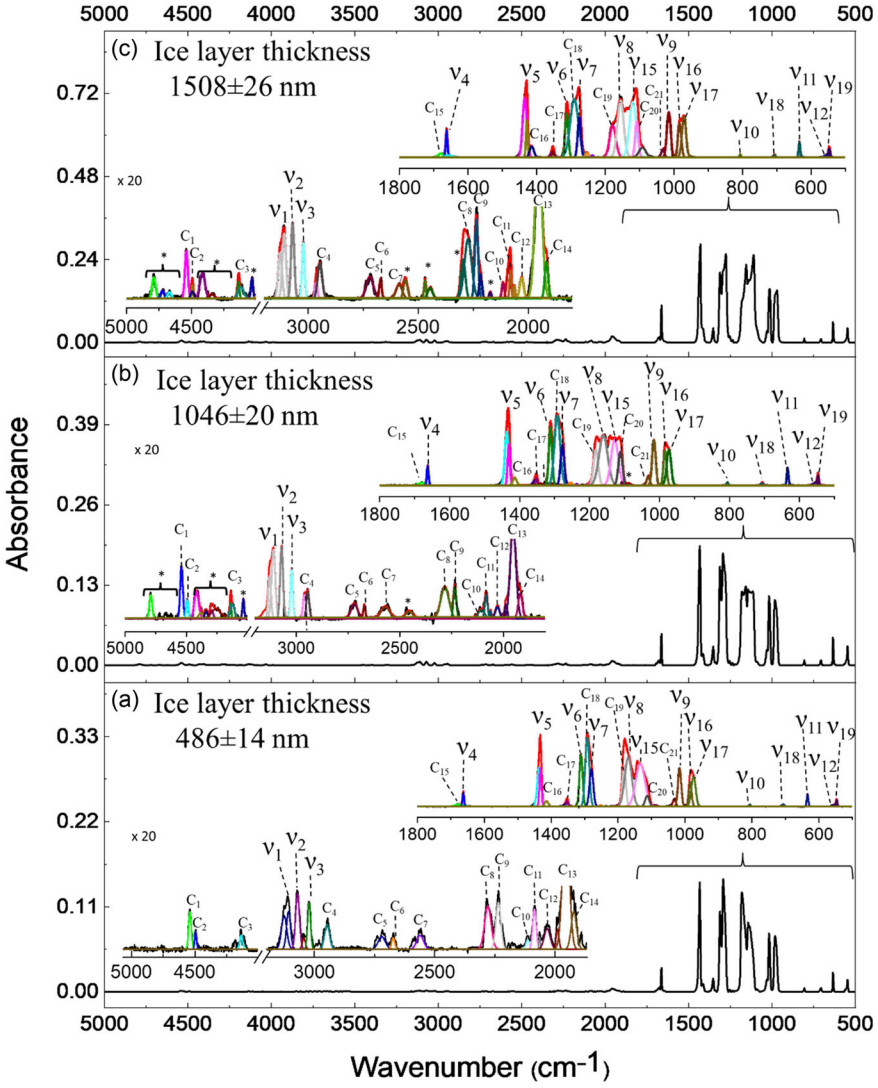

Figure 5. Infrared spectra of 3,3,3-trifluoropropene (R-III) at different ice thicknesses a) 486 ± 14 nm, b) 1046 ± 20 nm, and c) 1508 ± 26 nm.

Table 3. Number of fringes obtained from the laser interferometry for different thickness of refrigerant ices.

Name of the compound	Refractive index (η)	Number of fringes (n)	Thickness of ice (d) [nm]
1,1,1,2-Tetrafluoroethane (R-I)	1.24 ± 0.02	2.0 ± 0.1	518 ± 16
		4.1 ± 0.1	1037 ± 21
		6.1 ± 0.1	1556 ± 24
2,3,3,3-Tetrafluoropropene (R-II)	1.34 ± 0.02	2.1 ± 0.1	504 ± 15
		4.3 ± 0.1	1015 ± 18
		6.3 ± 0.1	1486 ± 21
3,3,3-Trifluoropropene (R-III)	1.30 ± 0.03	2.0 ± 0.1	486 ± 14
		4.3 ± 0.1	1046 ± 20
		6.2 ± 0.1	1508 ± 26

fundamental vibrational modes for spectral shifts and intensity changes with respect to the vapor-phase spectra as well as with ice layer thicknesses for each of the refrigerants. The fundamental and the combination/overtone modes of the refrigerants used in this study are represented in terms of ν_n (R-I/R-II/R-III) and C_n (R-I/R-II/R-III), respectively, where n is an integer number. As an example, first fundamental and combination modes of R-I are denoted as ν_1 (R-I) and C_1 (R-I), respectively. The combination

Table 4. Fundamental modes of 1,1,1,2-tetrafluoroethane (CF_3CH_2F) (R-I) and their respective band strength.

Fundamental modes assigned[a]	Experimental frequency 10 K[a] (cm^{-1})	Calculated frequency[a] (cm^{-1})	Band strength (10^{-18} cm molecule^{-1})	Solid-phase infrared frequency at 150 K[33] (cm^{-1})	Raman peak of liquid at 203 K[32,33] (cm^{-1})	Gas-phase infrared frequency at 298 K[a,34,35] (cm^{-1})	Assignment[a)35]
ν_{12}	3045	3125	0.08 ± 0.01		3030	3013	σ_{as} (CH_2)
ν_1	3002	3065	0.53 ± 0.06		2990	2986	σ_s (CH_2)
ν_2	1462	1495	0.73 ± 0.06			1464	β (CH_2) scissoring
ν_3	1429	1441	1.08 ± 0.08	1427		1427, 1419	$\omega(CH_2)/\sigma$ (CC)
ν_{13}	1301–1292	1306	2.63 ± 0.49			1301	β (CC)/τ (CH_2 out of plane)
ν_4	1283–1277	1289	1.20 ± 0.17	1279	1284	1299, 1292	$\omega(CH_2) + \delta_s(CF_3) + \sigma$ (CC)
ν_{14}	1192–1181	1194	3.18 ± 0.28			1203	ν_{as} (CF) + τ (CH_2 in plane)
ν_5	1166–1161	1160	1.76 ± 0.08	1167	1173	1189, 1182	σ_s (CF) + $\omega(CH_2)$
ν_6	1081, 1060	1103	1.06 ± 0.07	1069	1061	1070	σ (CF of CH_2F)/σ (CC)
ν_{15}	971	976	0.75 ± 0.23	965	968	972	$\rho(CH_2)$ + b (CF of CH_2F)
ν_7	841		0.49 ± 0.04	839	837	844, 847	$\sigma_s(CF_3)/\sigma$ (CC)
ν_8	664	664	0.72 ± 0.09	660	660	666, 658	$\delta_s(CF_3)/\delta(CH_2F)$
ν_9	550	550	0.20 ± 0.02	550	548	557	δ_s (CF_3)
ν_{16}	533	535	0.07 ± 0.01	534		542	δ_{as} (CF_3)
ν_{10}		418		411	407	410	δ_{as} (CF_3)/$\delta(CH_2F)$
ν_{17}		374		357	358	362, 354	$\rho(CF_3)/\rho(CH_2)$
ν_{11}		240				222	$\rho(CF_3)/\rho(CH_2F)$
ν_{18}		166		124		112	Torsion

ν, frequency; σ, stretching; β, bending; ρ, rocking; δ, deformation; ω, wagging; τ, twisting; s, symmetric; as, asymmetric; a, this study.

frequencies are marked from higher to lower frequency to avoid more complications (Table 7–9), and the fundamental modes are assigned according to previous studies as mentioned in Table 4–6.

3.2.1.1. Spectral Shifts and Intensity Alteration in Ices Compared to the Gas Phase

Vapor-deposited, low-temperature solid-phase infrared spectra of all the refrigerants used in this study induce significant changes in spectral intensity pattern and spectral shift in major fundamental vibrational modes with respect to their vapor-phase infrared spectra, as well as with the variation of the thickness of ice. Most of the HFCs have significant absorption in the 500–2000 cm^{-1} region corresponding to the most prominent fundamental modes. Infrared spectral changes at different thickness of ices with vapor-phase infrared spectra for each of the refrigerants in this region are compared in **Figure 6**a–c, and full infrared vapor-phase spectra are provided in Figure S4a–c, Supporting Information.

The C—F vibrational modes associated with the CF_3 group reveal the strongest absorptions among all vibrational modes irrespective of the nature of the refrigerant. Apart from these C—F stretching modes, R-I and R-II carry F atom bonded to sp^3 and sp^2 hybridized carbon atoms. In all cases, the C—F stretching modes are coupled with, e.g., CH_2 bending, C—C stretching, and C—C bending modes. Significantly, the CH_2 bending modes such as scissoring and wagging – coupled with C—C stretching and C—C bending—do not exhibit any spectral shifts when between the gas-phase spectra and ices. As an example in case of (R-I), the vibrational modes associated with CH_2 scissoring contributed with C—C bending (ν_2 (R-I): 1462 cm^{-1}) and CH_2 wagging (ω) contributed with C—C stretching (ν_3 (R–I): 1429 cm^{-1}) does not exhibit spectral shifts. However, there is an increase in relative intensity of these modes in the solid phase compared to the gas phase indicating amorphous morphology in solid phase affecting modes with respect to gas phase, which needs further theoretical calculation to get further insights. A similar trend is also observed in the case of olefinic HFCs (HFO), but apart from the CH_2 bending modes, C—C vibrational modes associated with the C=C moiety are also observed. In all cases, the C=C stretching modes do not show spectral shifts with respect to the gas-phase spectra or distinct ice thicknesses. However, the individual spectral position of the C=C stretching modes is distinct. The C=C stretching mode for 2,3,3,3-tetrafluoro propene (R-1234yf), where a fluorine atom is bonded to the olefine, is at higher frequency (ν_3(R-II): 1701 cm^{-1}) compared to same C=C (ν_5 (R-III): 1662 cm^{-1}) for 3,3,3-trifluoropropene (R-III), where no fluorine atom is bonded to the olefinic moiety. Besides the increase in the stretching frequency, a similar trend is noticeable for the relative intensities of the C=C modes, which indicates bonding with a fluorine atom to the carbon–carbon double bond induces larger changes in the dipole moment. The following section describes

Table 5. Fundamental modes of 2,3,3,3-tetrafluoropropene ($CF_3CF{=}CH_2$) (R-II) and their respective band strength.

Fundamental modes assigned[a]	Experimental frequency 10 K[a] (cm^{-1})	Calculated frequency[a] (cm^{-1})	Band strength (10^{-18} cm molecule^{-1})	Solid-phase Raman frequency 150 K[36,37]	Raman liquid 203 K[36,37]	Gas-phase infrared frequency 298 K[a,36,37]	Assignment[a,36]
ν_1	3159	3280	0.48 ± 0.06	3160	3158	3161	σ_{as} (CH_2)
ν_2	3052	3181	0.29 ± 0.04	3037	3036	3055	σ_s (CH_2)
ν_3	1700	1751	1.27 ± 0.08	1700	1698	1700	σ (C=C)
ν_4	1395	1359	1.17 ± 0.41	1390	1388	1391	ρ(CH_2)/σ_{as} (CF_3)
ν_5	1365, 1350 (PR)		0.83 ± 0.07	1347	1352	1357	σ (C—F of alkene)/β (C—C)
ν_6	1200–1205	1184	0.68 ± 0.05	1192	1208	1210	σ_{as} (CF_3)/β (CH_2) scissoring/β (C—F of alkene)
ν_{15}	1173–1166	1155	2.74 ± 0.29	1161	1162	1181	δ_s (CF_3)/σ (C—F of alkene)/ρ(CH_2)
ν_7	1137–1162	1148	0.87 ± 0.07	1134		1162	σ_s (CF_3)/τ (CH_2)
ν_8	939	961	0.68 ± 0.04	938	942	945	ρ(CH_2)/σ (C—F of alkene)
ν_{16}	914-901	929	0.99 ± 0.18	910	902	889	ω(CH_2)/β (C=C)
ν_9	789	786	0.11 ± 0.01	790	790	793	σ (C—C)/ρ(CH_2)/δ_s(CF_3)
ν_{10}	615	611	0.22 ± 0.04	614	616	615	δ (CCF) in plane/ρ(CH_2)
ν_{11}	575	571	0.13 ± 0.01	576	576	579	δ_s(CF_3)/ρ(CH_2)
ν_{19}		493		497	497		δ_{as} (CF_3)/τ (CH_2)/δ (CCF) out of plane
ν_{12}		415		423	421		δ (CCC) in plane
ν_{13}		370		370	367		δ(C=C—F) in plane
ν_{20}		240		237	239		δ (CF_3)

ν, frequency; σ, stretching; β, bending; ρ, rocking; δ, deformation; ω, wagging; τ, twisting; s, symmetric; as, asymmetric; a, this study.

Table 6. Fundamental modes of 3,3,3-trifluoropropene ($CF_3CH{=}CH_2$) (R-III) and their respective band strength.

Fundamental mode assigned[a]	Experimental frequency 10 K[a] (cm^{-1})	Calculated frequency[a] (cm^{-1})	Band strength (10^{-18} cm molecule^{-1})	Solid-phase infrared frequency 150 K[38]	Raman liquid 203 K[38]	Gas-phase infrared frequency 298 K[a,a,39,40]	Assignment[a,39,40]
ν_1	3125, 3110	3244	0.06 ± 0.01	3113	3127	3124	σ_{as} (CH_2)
ν_2	3070	3188	0.06 ± 0.01	3073	3066	3066	σ (CH adjacent to CF_3)
ν_3	3022	3155	0.04 ± 0.01	3021	3021	3016	σ_s (CH_2)
ν_4	1662	1723	0.28 ± 0.02	1673	1662	1671	σ (C=C)
ν_5	1432	1461	0.47 ± 0.09	1429	1432	1433	β (CH_2) scissoring/β (C=CH)/β (C—C)
ν_6	1311	1329	0.99 ± 0.15	1313	1312	1311	ρ(HC=CH)/δ_s (CF_3)
ν_7	1276–1280	1282	0.86 ± 0.17	1285	1284	1285	σ_{as} (CF_3)/ρ(HC=CH)/β(C—C)
ν_8	1152–1168	1164	2.41 ± 0.26	1183	1169	1182	σ_{as} (CF_3)/ρ (HCH)/δ (C=C—C) in plane
ν_{15}	1119–1133	1125	2.35 ± 0.35	1156	1143	1160	σ_{as} (CF_3)/τ (HCH) in plane/δ (C=C—C) out of plane
ν_9	1016	1031	0.80 ± 0.20	1009	1017	1021	ρ (CH_2)/δ (C=C—C) in plane
ν_{16}	984	1016	0.79 ± 0.08	980	968	980	τ (HCH) out of plane/τ (HC=CH) out of plane
ν_{17}	974	1002	0.93 ± 0.14	963	960	889	ω(CH_2)/δ (HC=C) out of plane
ν_{10}	806	806	0.03 ± 0.01	805	808	810	σ_s (CF_3)/β (HC=C) in plane/ρ(CH_2)
ν_{18}	706	719	0.09 ± 0.01	700	708	705	σ_s (CF_3)/β (HC=C) out of plane/ρ(CH_2) [ν_{18}]
ν_{11}	634	611	0.08 ± 0.01	614	616	615	δ (CCF) in plane/ρ(CH_2)
ν_{12}	554	541	0.09 ± 0.01	556	547	553	δ_{as} (CF_3)/τ (HCH) out of plane/σ (C—C)/δ (C=C—C) in plane
ν_{19}	546	511	0.09 ± 0.01	544	521	543	δ_{as} (CF_3)/δ(C=C—C) out of plane
ν_{13}		429		423	432	431	β (C=C—C) in plane/ρ (CF_3)
ν_{20}		314		320	312	317	β (C=C—C) out of plane + ρ (CF_3)
ν_{14}		279		237	239		ρ (CF_3)

ν, frequency; σ, stretching; β, bending; ρ, rocking; δ, deformation; ω, wagging; τ, twisting; s, symmetric; as, asymmetric; a, this study.

Table 7. Combination modes of 1,1,1,2-tetrafluoroethane (CF_3CH_2F) (R-I) and their respective band strength.

Combination modes assigned[a]	Experimental frequency 10 K[a] (cm^{-1})	Band strength (10^{-19} cm molecule^{-1})	Solid-phase infrared frequency 150 K	Raman liquid 203 K[33]	Gas-phase infrared frequency 298 K[b]	Assignment[a]
C_1	4475	1.50 ± 0.14				$\nu_{12} + \nu_2$
C_2	4436	0.24 ± 0.04				$\nu_1 + \nu_2$
C_3	2910	0.62 ± 0.06			2912	$2\nu_2$
C_4	2885	0.24 ± 0.02			2887	$\nu_2 + \nu_3$
C_5	2586	0.32 ± 0.01				$\nu_{13} + \nu_4$
C_6	2469	0.74 ± 0.02				$\nu_4 + \nu_{14}$
C_7	2417	0.32 ± 0.07			2424	$\nu_2 + \nu_{15}$
C_8	2396	0.29 ± 0.01				$\nu_{13} + \nu_{15}$
C_9	2354	0.63 ± 0.07			2359	$\nu_4 + \nu_6$
C_{10}	2267	0.48 ± 0.07			2267	$\nu_4 + \nu_{15}$
C_{11}	2253	0.88 ± 0.02				$\nu_5 + \nu_{15}$
C_{12}	2129	1.71 ± 0.05			2137	$2\nu_6$
C_{13}	2010	0.42 ± 0.01				$\nu_2 + \nu_9$
C_{14}	1930	0.35 ± 0.01			1945	$2\nu_{15}$
C_{15}	1832	0.91 ± 0.10			1831	$\nu_3 + \nu_{10}$
C_{16}	1390	1.65 ± 0.15	1386	1389	1382	$\nu_7 + \nu_{16}$
C_{17}	1374	2.09 ± 0.19	1372		1374	$\nu_{10} + \nu_{15}$
C_{18}	1249	1.05 ± 0.03				$\nu_{15} + \nu_{17}$
C_{19}	1210	11.82 ± 1.51				$\nu_8 + \nu_{16}$
C_{20}	820	0.39 ± 0.01	820			$2\nu_{10}$
C_{21}	687	1.09 ± 0.03			673	$\nu_{10} + \nu_{11}$

distinct C—F vibrational modes coupled with associated modes in terms of vibrational shifts, intensities, and spectral broadening for the refrigerants used in this study.

Apart from the existence of vibrational shifts of refrigerant ice at 10 K with respect to gas-phase spectra, change in spectral pattern corresponding to C—F vibrational modes within the region 2000 cm^{-1} to 500 cm^{-1} also has been observed at 80 K for non-olefinic refrigerant 1,1,1,2-tetrafluoroethane and at 70 K for rest of the olefinic refrigerants (2,3,3,3-tetrafluoropropene and 3,3,3-trifluoropropene), indicating formation of crystalline phase.[53,54] As the primary objective of this study is to quantify optical spectroscopic parameter and understanding vibrational shifts, variation in spectral pattern due to phase shift are provided in S5a–c, Supporting Information as a general observation during sublimation of refrigerant ices. However, further combined experimental and theoretical study in this direction could stipulate further insights toward the phase transition of the refrigerants used in this study.

3.2.1.2. 1,1,1,2-Tetrafluoroethane (CF_3CH_2F) (R-I)

The most intense C—F vibrational modes along with C—H and C—C modes likely remain in the 1328 cm^{-1} to 1260 cm^{-1} and 1238 cm^{-1} to 1154 cm^{-1} regions; the first region corresponds to fundamental modes of CH_2 wagging (ω) having contributions from the C—C stretching (σ) and CF_3 deformation (δ_{CF3}), while the second region corresponds to CF_3 stretching (σ_{CF3}) fundamentals with contributions from C—H and C—C bending modes (Figure 6a). These fundamental modes, in which contribution from C—F vibrational mode exists, induce a frequency redshift in the solid ices as compared to vapor phase due to intermolecular interactions through in F···H. For example, fundamental CF_3 stretching mode in the ices (ν_5 (R-I)) undergoes a redshift from 1184 cm^{-1} in the gas phase to 1161 cm^{-1} for the 1556 ± 24 nm thick ice. The concerned mode has a contribution from CH_2 wagging (ω). On the other hand, the fundamental CH_2 wagging (ω) (ν_4 (R-I)) is also red shifted from 1292 cm^{-1} in the gas phase to 1283 cm^{-1} in the ice of 518 ± 16 nm thickness, which is further red shifted toward 1277 cm^{-1} for a thicker ice of 1556 ± 24 nm due to significant contribution of CF_3 deformation (δ_{CF3}) mode, which usually undergoes spectral redshift as mentioned earlier. Apart from the modes associated with the contribution from C—F vibrations arising from CF_3, C—F vibration arising from adjacent CH_2F moiety also induces frequency red shifting in the solid ices as compared to vapor phase.

Although the extent of redshift is more dominant involving this C—F vibration (30 cm^{-1}) compared to the other originated from CF_3 (15–20 cm^{-1}). The extent of redshift remains same with the increase of ice thickness, which indicates this C—F stretching is not affected with layer of ice formation. The other low frequency modes in the ices below 1000 cm^{-1} region do not show any significant redshifts with respect to the gas-phase spectra.

Table 8. Combination modes of 2,3,3,3-tetrafluoropropene ($CF_3CF{=}CH_2$) (R-II) and their respective band strength.

Combination modes assigned[a]	Experimental frequency 10 K[a] (cm^{-1})	Band strength (10^{-19} cm molecule^{-1})	Solid-phase Raman frequency 150 K[37]	Gas-phase infrared frequency 298 K[a,36]	Assignment[a]
C_1	4497	0.58 ± 0.04		4503	$\nu_1 + \nu_5$
C_2	4292	0.23 ± 0.05		4305	$\nu_1 + \nu_6$
C_3	4091	0.46 ± 0.05		4100	$\nu_1 + \nu_8$
C_4	3387	0.64 ± 0.06		3393	$2\nu_3$
C_5	3093	0.68 ± 0.10	3094	3096	$\nu_3 + \nu_4$
C_6	3062	1.81 ± 0.31	3062	3070	$\nu_3 + \nu_9 + \nu_{11}$
C_7	2740	0.15 ± 0.04		2749	$\nu_4 + \nu_5$
C_8	2700	0.09 ± 0.01		2708	$2\nu_5$
C_9	2631	0.48 ± 0.10		2644	$\nu_3 + \nu_8$
C_{10}	2596	0.23 ± 0.03			$\nu_4 + \nu_6$
C_{11}	2555	0.17 ± 0.02			$\nu_4 + \nu_{15}$
C_{12}	2485	0.05 ± 0.01			$\nu_3 + \nu_9$
C_{13}	2195	0.14 ± 0.02		2202	$\nu_4 + \nu_9$
C_{14}	2177	0.19 ± 0.05		2180	$\nu_5 + \nu_9$
C_{15}	2139	0.23 ± 0.01		2146	$\nu_5 + \nu_9$
C_{16}	2077	0.24 ± 0.05		2099	$\nu_5 + \nu_8$
C_{17}	1982	0.31 ± 0.02		1996	$\nu_3 + \nu_{10}$
C_{18}	1936	0.55 ± 0.10		1943	$\nu_{15} + \nu_7$
C_{19}	1876	0.87 ± 0.12		1893	$2\nu_{11} + \nu_9$
C_{20}	1815	0.95 ± 0.11		1823	$2\nu_8$
C_{21}	1406	13.01 ± 0.08	1408		β (CH_2) scissoring + (C—C) bending
C_{22}	1334	0.78 ± 0.10		1356	$\nu_8 + \nu_{16}$
C_{23}	1285	0.76 ± 0.04		1291	$\nu_9 + \nu_{11}$
C_{24}	1224	12.45 ± 1.51			$\nu_{12} + \nu_{16}$
C_{25}	1133–1125	2.24 ± 0.10		1114	$2\nu_{11}$
C_{26}	1086	1.45 ± 0.15		1088	$\nu_{11} + \nu_{19}$

3.2.1.3. 2,3,3,3-Tetrafluoropropene ($CF_3CF{=}CH_2$) (R-II)

This new-generation HFO is a quite distinct as R-II carries a fluorine atom at the olefinic (C=C) moiety. The presence of this fluorine induces significant coupling with the C=C group leading to closely associated vibrational modes even in gas phase unlike R-I (Figure 6b). Most of the fundamental CH_2 bending modes like rocking (ρ) and twisting (τ) not only have contribution from the C—F stretching and bending modes originating from CF_3 but also from the C—F moiety of the sp^2 hybridized carbon atom. Although the modes are closely associated, the vibrational mode ν_{15} (R-II) consisting C—F stretching of olefinic-bounded CF along with other modes CH_2 scissoring and C—F deformation (δ_{CF3}) of CF_3 exhibits same extent of red shifting in different thickness of solid ices (1170 cm^{-1}) compared to the gas-phase spectra (1181 cm^{-1}) like to the case of R-I. On the other hand, increase in redshift with the extent of ice thickness compared to gas phase in the case of ν_6 (R-II) and ν_7 (R-II) fundamental mode, carrying symmetric and asymmetric C—F stretching of CF_3 group, indicates involvement of C—F stretching of CF_3 in ice layer formation via intermolecular H-bonding interactions, weakening the C—F bond.

In addition to the modes similar to R-I, this olefinic refrigerant has C=C—F vibrations (stretching or bending), which exhibit two distinct modes with respect to the molecular plane: in plane and out of plane. Distinct spectral shifts are observed within two fundamental modes ν_8 (R-II) & ν_{16} (R-II) in the ices as compared to the gas-phase spectra. The first mode, where the fundamental CH_2 rocking (ρ) mode has contribution from the in-plane C=C—F vibration, experiences a redshift from 949 cm^{-1} to 939 cm^{-1}, while the second mode exhibits an unusual blue shift from 890 cm^{-1} to 910 cm^{-1}; here, along with the CH_2 wagging (ω) fundamental mode contribution from out of plane C=C—F vibrational mode exists. However, both modes are not further red or blue shifted with increasing thicknesses of the ice layers. This unusual blue shift of CH_2 wagging (ω) fundamental mode possibly occurred due to repulsive interaction.[55,56]

Table 9. Combination modes of 3,3,3-trifluoropropene ($CF_3CF{=}CH_2$) (R-III) and their respective band strength.

Combination modes assigned[a]	Experimental frequency 10 K[a] (cm^{-1})	Band strength (10^{-19} cm molecule^{-1})	Assignment[a]
C_1	4541	0.70 ± 0.06	$\nu_1 + \nu_5$
C_2	4489	0.14 ± 0.03	$\nu_1 + \nu_6$
C_3	4133	0.14 ± 0.01	$\nu_1 + \nu_{15}$
C_4	2944	0.39 ± 0.08	$\nu_4 + \nu_6$
C_5	2714	0.38 ± 0.06	$\nu_4 + \nu_{15}$
C_6	2669	0.11 ± 0.05	$\nu_5 + \nu_7$
C_7	2560	0.26 ± 0.02	$\nu_5 + \nu_{15}$
C_8	2282	1.05 ± 0.17	$\nu_7 + \nu_9$
C_9	2237	0.61 ± 0.15	$\nu_8 + \nu_{15}$
C_{10}	2116	0.17 ± 0.03	$\nu_9 + \nu_{16}$
C_{11}	2087	0.30 ± 0.01	$\nu_7 + \nu_{10}$
C_{12}	2031	0.21 ± 0.03	$\nu_{15} + \nu_{17}$
C_{13}	1952	2.60 ± 0.18	$\nu_{16} + \nu_{17}$
C_{14}	1919	0.35 ± 0.02	$2\nu_{17}$
C_{15}	1675	1.25 ± 0.18	$\nu_{16} + \nu_{11}$
C_{16}	1411	2.43 ± 0.35	$\nu_{13} + \nu_{17}$
C_{17}	1352	1.36 ± 0.05	$\nu_{10} + \nu_{20}$
C_{18}	1294	27.83 ± 1.91	$\nu_{11} + \nu_{19}$
C_{19}	1181	11.73 ± 1.03	$\nu_{10} + \nu_{12}$
C_{20}	1114	7.39 ± 0.64	$2\nu_{12}$
C_{21}	1034	1.26 ± 0.40	$\nu_{11} + \nu_{13}$

3.2.1.4. 3,3,3-Trifluoropropene ($CF_3CH{=}CH_2$) (R-III)

This simple HFO shows similar thermodynamic property with R-II, but when structurally compared with R-II, this refrigerant does not carry any olefinic bounded fluorine atom. The C—F vibrations for R-III originates from CF_3 group only. The absence of the olefine bonded fluorine atom induces less coupling between the vibrational modes, which is evident from the experimentally measured vapor-phase vibrational spectra of R-II and R-III. Most of the CF_3 fundamental vibrational modes remain mixed with olefinic modes such as HC=CH bending and C=C—C bending (Figure 6c and Table 6). All C—F stretching fundamental modes experience redshifts in the solid-phase spectra. The HC=CH bending mode coupled with C—F stretching fundamental mode (ν_7 (R-III)) reveal redshifts (1280–1276 cm^{-1}) compared to gas phase (1285 cm^{-1}) as evident from Figure 6c. The olefinic C=C—C moiety has two type of modes as in-plane and out-of-plane, which contribute to the fundamental CF_3 stretching and generate two types of CF_3 stretching ν_8 (R-III) and ν_{15} (R-III), respectively. These modes are redshifted in solid ices as compared to vapor phase like all other cases. Apart from the C=C—C vibration, the C=C—H moiety results in similar vibrations like the C=C—F moiety in R-II. The out-of-plane C=C—H contributed fundamental mode of CH_2 wagging (ω) (ν_{17} (R-III) exhibits blue shifts, as in the case of R-II, due to the formation of a less mobile, regular lattice structure. However, the extent of these blue shifts is lower compared to R-II due to the absence of directly bound F induces less steric repulsion.

3.2.2. Infrared Band Strength Measurements

The infrared spectroscopic data are key for the quantification of upper tropospheric species either in the form of gas, liquid, or solid. Infrared intensities of low-temperature ices are quantified in terms of band strengths (in cm molecule^{-1}). Experimentally measured integrated absorbances ($\int A d\nu$) are utilized to evaluate the band strengths as they are related through Equation (6)[57,58] where ρ = mass density; N_A = Avogadro number; M = molar mass; L = optical path length, and A' = band strength.

$$\int A d\nu = \left(\frac{\rho N_A A'}{2.303M}\right) L \tag{6}$$

In our measurements, densities of R-I, R-II, and R-III are taken from crystallographic data at low temperatures. Both R-I and R-II forms body-centered cubic (bcc) lattice with density 1.77 g cm^{-3} and 1.74 g cm^{-3} respectively.[37,59] Both R-I and R-II contain a CF_3 group. In case of R-III, low-temperature crystallographic data are not available best to our knowledge and since it also contains

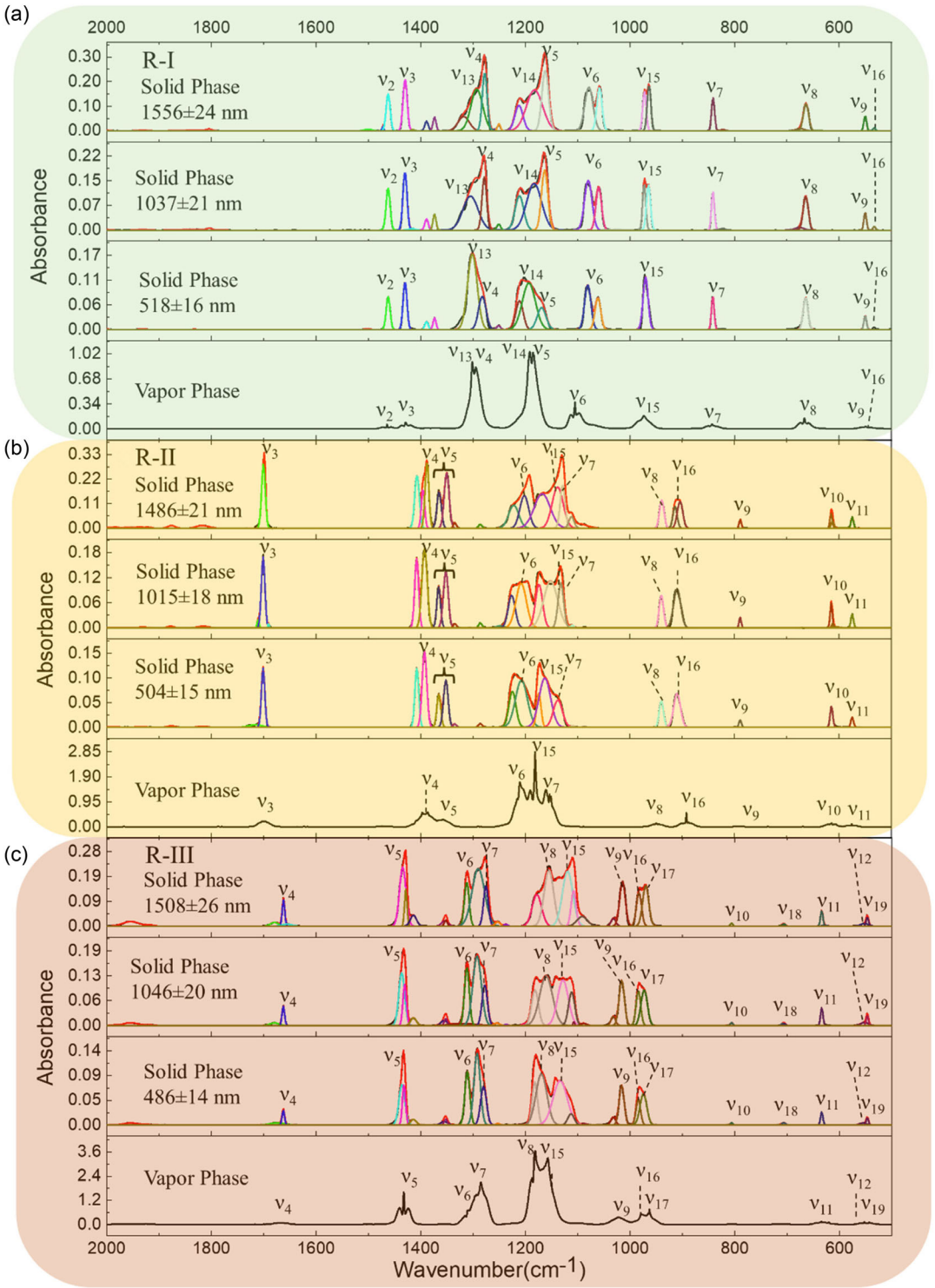

Figure 6. Comparison of infrared spectra of the refrigerants in the vapor phase and solid phase experimentally measured in this study. a) 1,1,1,2-Tetrafluoroethane (R-I) at ice thicknesses of 518 ± 16 nm, 1037 ± 21 nm, 1556 ± 24 nm; b) 2,3,3,3-tetrafluoropropene (R-II) at ice thicknesses of 504 ± 15 nm, 1015 ± 18 nm, 1486 ± 21 nm; c) 3,3,3-trifluoropropene (R-III) at thicknesses of 486 ± 14 nm, 1046 ± 20 nm, 1508 ± 26 nm.

CF_3 group the density of R-III is considered as average density of functionally similar R-I and R-II.

Unlike the gas-phase infrared spectra, spectra of solid ices are broad with widths exceeding 4 cm^{-1}. Experimentally measured spectra were analyzed through deconvolution. The integrated areas of the deconvoluted peaks were plotted versus the optical path length (L) to determine band strengths from the slope as described in Equation (6). The plots of the integrated area versus

optical path length (L) are nearly linear. A plot of integrated area with respect to path length (L) for R-I is provided as a representative in Figure S6, Supporting Information. The band strengths of the fundamental bands determined through the analysis are provided in Table 4–6. Similarly, Table 7–9 provides band strengths for the infrared analysis of combination bands. From the analysis of the band strengths, it is quite evident that the most intense frequency among all the frequencies for all refrigerants is C—F vibrational (bending or stretching) modes originating from CF_3. In case R-I CF_3 deformation contributed CH_2 twisting mode ν_{14} (R-I) within 1180–1191 cm^{-1} is the strongest having band strength (A') of $3.18 \pm 0.28 \times 10^{-18}$ cm $molecule^{-1}$. However, in case of R-II, due to enhanced coupling with F atom directly bound to C=C moiety, the highest intensity vibrational mode corresponds to C—F stretching mode originating from olefine bound F. Thus, ν_{15} (R-II) is the strongest one having band strength of $2.74 \pm 0.29 \times 10^{-18}$ cm $molecule^{-1}$. Another olefin that does not contain directly bound F with olefine has the highest band strength for the vibrational mode ν_8 (R-III) where asymmetric CF_3 stretch is coupled with CH_2 and C=C—C bending.

4. Conclusion

Refrigerant recycling, purification, and low-temperature molecular interactions of refrigerants in the upper troposphere represent fundamental physico-chemical processes. Laboratory experiments require key optical and spectroscopic parameters, such as refractive indices and band strengths, which are often absent at low temperatures. Here, experimentally measured refractive indices of important refrigerants 1,1,1,2-tetrafluoroethane (CF_3CH_2F; HFC134a), 2,3,3,3-tetrafluoropropene ($CF_3CF{=}CH_2$; R1234yf), and 3,3,3-trifluoropropene ($CF_3CH{=}CH_2$; R1243zf) were evaluated to be 1.24 ± 0.02, 1.34 ± 0.02, and 1.30 ± 0.02, respectively. Further, the analysis of vibrational assignments of HFCs was well supported by electronic structure calculations. The reliability of the computational method is benchmarked by comparing the calculated frequencies with those obtained experimentally. Calibration factors are calculated to be 0.983 ± 0.001, 1.004 ± 0.001, and 0.981 ± 0.001 for CF_3CH_2F, $CF_3CF{=}CH_2$, and $CF_3CH{=}CH_2$, respectively. All HFCs carry a CF_3 group, which typically contributes the most intense vibrational mode, with band strengths in the range of 2×10^{-18} to 3×10^{-18} cm $molecule^{-1}$. However, in the olefine 2,3,3,3-tetrafluoropropene (R-1234yf) (R-II), the strongest vibration originates from olefine bound C—F bond. The optical parameter refractive index (η_R) and band strength (A') are interrelated, as optical pathlength (L) which used in the determination of band strength (A') is related dependent on refractive index (η_R) through Equation (2)–(4). A comparison of the solid-state spectra with the gas-phase infrared spectra reveals that most of the C—F stretching frequencies are redshifted. Overall, through our quantitative investigation of key optical and spectroscopic parameters, an unexplored yet essential inventory to understand low-temperature data of HFCs were collected and presented. Apart from that amorphous to crystalline phased transformations are also evidenced exploiting absorption reflection absorption infrared spectroscopy, further theoretical calculation could provide further insights toward evidenced phase transitions.

Supporting Information

Calibration of calculated frequency with experimental ones (Figure S1); experimentally measured interference patterns for methane (Figure S2); interference patterns of different refrigerants observed during deposition (Figure S3); combination bands arise at higher thicknesses of refrigerant ices (Table S1); optimized coordinates of the refrigerants (Table S2); experimentally measured vapor-phase infrared spectra of the refrigerants (Figure S4); evidence of crystalline phase transformation at elevated temperature (Figure S5); and representative plot of integrated areas versus ice thicknesses utilized to measure band strengths (Figure S6).

Acknowledgements

This study was funded through the NSF award, 2330175, Center: NSF Engineering Research Center for Environmentally Applied Refrigerant Technology Hub.

Conflict of Interest

The authors declare no conflict of interest.

Data Availability Statement

All the data are included in the manuscript and/or supporting information.

Keywords: infrared spectroscopy · interferometry · low temperatures · refrigerants · solids

[1] F. Pardo, G. Zarca, A. Urtiaga, *ACS Sustain. Chem. Eng.* **2020**, *8*, 2548.
[2] P. Dewapriya, L. Chadwick, S. G. Gorji, B. Schulze, S. Valsecchi, S. Samanipour, K. V. Thomas, S. L. Kaserzon, *J. Hazard. Mater. Lett.* **2023**, *4*, 100086.
[3] D. W. Phelps, L. V. Parkinson, J. M. Boucher, J. Muncke, B. Geueke, *Environ. Sci. Technol.* **2024**, *58*, 5670.
[4] S. Hamlin, R. Hunt, S. Tassou, *Appl. Therm. Eng.* **1998**, *18*, 1139.
[5] X. Liu, T. Zhang, Q. Gao, X. Xu, H. Chen, S. Wang, *Appl. Therm. Eng.* **2024**, *236*, 121613.
[6] Z. Zhou, B. Chen, Y. Wang, L. Guo, G. Wang, *Appl. Therm. Eng.* **2012**, *39*, 29.
[7] K. N. Taddonio, G. B. Dreyfus, S. O. Andersen, A. Ravishankara, *Environ. Sci. Technol.* **2023**, *57*, 11731.
[8] T. Tan, L. Rennels, B. Parthum, *Nat. Clim. Chang.* **2024**, *14*, 55.
[9] B. K. Sovacool, S. Griffiths, J. Kim, M. Bazilian, *Renew. Sustain. Energy Rev.* **2021**, 141.
[10] A. K. Vuppaladadiyam, E. Antunes, S. S. V. Vuppaladadiyam, Z. T. Baig, A. Subiantoro, G. Lei, S.-Y. Leu, A. K. Sarmah, H. Duan, *Sci. Total Environ.* **2022**, *823*, 153670.

[11] F. Graziosi, J. Arduini, F. Furlani, U. Giostra, P. Cristofanelli, X. Fang, O. Hermanssen, C. Lunder, G. Maenhout, S. O'Doherty, *Atmos. Environ.* **2017**, *158*, 85.
[12] S. Xiaopu, W. Pu, L. Hui, G. Bai-He, W. Yi, *Adv. Clim. Change Res.* **2022**, *13*, 564.
[13] X. Ruan, Y. Dai, L. Du, X. Yan, G. He, B. Li, *Sep. Purif. Technol.* **2015**, *156*, 673.
[14] H. B. et al., Perfluorocompound separation and purification method and system. US- 5779863-A, 1998-07-14 **1998**.
[15] M. W. T. et al., Reclamation and separation of perfluorocarbons using condensation. US-6383257-B1, 2002-05-07 **2002**.
[16] W. M. Drout, Extractive distillation process. US-2610141-A, 1952-09-09 **1952**.
[17] Z. Lei, C. Li, B. Chen, *Sep. Purif. Rev.* **2003**, *32*, 121.
[18] E. A. Finberg, M. B. Shiflett, *Ind. Eng. Chem. Res.* **2021**, *60*, 16054.
[19] A. Mota-Babiloni, M. M. Joybari, J. Navarro-Esbrí, C. Mateu-Royo, Á. Barragán-Cervera, M. Amat-Albuixech, F. Molés, *Int. J. Refrig.* **2020**, *111*, 147.
[20] Í. F. Guilherme, D. F. M. Pico, D. D. O. dos Santos, E. P. Bandarra Filho, *J. Build. Eng.* **2022**, *47*, 103847.
[21] L. Wang, P. Jiao, C. Dang, E. Hihara, B. Dai, *Int. J. Therm. Sci.* **2021**, *170*, 107090.
[22] V. Nair, *Int. J. Refrig.* **2021**, *122*, 156.
[23] X. Zhang, Y. Li, *Energy* **2024**, *311*, 133423.
[24] G. Salierno, *Chem. Sus. Chem* **2024**, *17*, e202400280.
[25] R. Holland, M. A. H. Khan, I. Driscoll, R. Chhantyal-Pun, R. G. Derwent, C. A. Taatjes, A. J. Orr-Ewing, C. J. Percival, D. E. Shallcross, *ACS Earth Space Chem.* **2021**, *5*, 849.
[26] J. B. Burkholder, R. Cox, A. Ravishankara, *Chem. Rev.* **2015**, *115*, 3704.
[27] S. Biswas, D. Paul, K. Mondal, R. I. Kaiser, *Proc. Natl. Acad. Sci.* **2025**, *122*, e2425543122.
[28] K. Mondal, S. Biswas, N. Melbourne, R. Sun, R. I. Kaiser, *Chem. Sci.* **2025**, *16*, 11039.
[29] G. E. Morales-Espejel, R. Meeuwenoord, A. F. Quiñonez, R. Hauleitner, *Proc. Inst. Mech. Eng. Part C J. Mech. Eng. Sci.* **2015**, *229*, 244.
[30] R. Morse, T. Moreira, J. Chan, K. Dressler, G. Ribatski, E. Hurlburt, L. McCarroll, G. Nellis, A. Berson, *Int. J. Heat Mass Transf.* **2021**, *177*, 121487.
[31] S. Kong, Z. Wang, X. Xu, H. Sun, Z. Liu, Y. Fang, M. Su, H. Yang, *Int. J. Multiph. Flow* **2022**, *153*, 104108.
[32] J. R. Nielsen, C. Halley, *J. Mol. Spectrosc.* **1965**, *17*, 341.
[33] W. F. Edgell, T. R. Riethof, C. Ward, *J. Mol. Spectrosc.* **1963**, *11*, 92.
[34] D. Harnish, R. Hirschmann, *Appl. Spectrosc.* **1970**, *24*, 28.
[35] L.-H. Xu, A. M. Andrews, R. R. Cavanagh, G. T. Fraser, K. K. Irikura, F. J. Lovas, J.-U. Grabow, W. Stahl, M. K. Crawford, R. J. Smalley, *J. Phys. Chem. A* **1997**, *101*, 2288.
[36] A. P. Charmet, L. Bizzocchi, B. M. Giuliano, P. Caselli, N. C. Craig, S. V. Krasnoshchekov, *J. Quant. Spectrosc. Radiat. Transf.* **2019**, *239*, 106656.
[37] M. Feller, K. Lux, C. Hohenstein, A. Kornath, *Z. Naturforsch. B* **2014**, *69*, 379.
[38] D. Christen, V. Hoffmann, P. Klaeboe, *Z. Naturforsch. A* **1979**, *34*, 1320.
[39] G. A. Guirgis, H. Zhen, J. B. Robb II, J. R. Durig, *Vib. Spectrosc.* **2000**, *23*, 137.
[40] A. Ainetschian, G. T. Fraser, B. H. Pate, R. Suenram, *Chem. Phys.* **1995**, *190*, 231.
[41] A. M. Turner, M. J. Abplanalp, R. I. Kaiser, *Astrophys. J.* **2016**, *819*, 97.
[42] M. McAnally, J. Bocková, A. M. Turner, N. Hara, D. Mikhnova, C. Meinert, R. I. Kaiser, *Proc. Natl. Acad. Sci.* **2025**, *122*, e2501839122.
[43] C. Zhu, A. M. Turner, M. J. Abplanalp, R. I. Kaiser, B. Webb, G. Siuzdak, R. C. Fortenberry, *Astrophys. J. Lett.* **2020**, *899*, L3.
[44] A. M. Turner, M. J. Abplanalp, A. Bergantini, R. Frigge, C. Zhu, B.-J. Sun, C.-T. Hsiao, A. H. Chang, C. Meinert, R. I. Kaiser, *Sci. Adv.* **2019**, *5*, eaaw4307.
[45] A. M. Turner, A. Bergantini, M. J. Abplanalp, C. Zhu, S. Góbi, B.-J. Sun, K.-H. Chao, A. H. Chang, C. Meinert, R. I. Kaiser, *Nat. Commun.* **2018**, *9*, 3851.
[46] A. U. Aldiyarov, D. Y. Sokolov, A. Y. Nurmukan, M. A. Ramos, *ACS Omega* **2020**, *5*, 11671.
[47] M. Domingo Beltrán, R. Luna Molina, M. Á. Satorre Aznar, C. Santonja Moltó, C. Millán Verdú, *Sensors* **2015**, *15*, 25123.
[48] E. Apra, E. J. Bylaska, W. A. De Jong, N. Govind, K. Kowalski, T. P. Straatsma, M. Valiev, H. J. van Dam, Y. Alexeev, J. Anchell, *J. Chem. Phys.* **2020**, 152.
[49] M. W. Wong, *Chem. Phys. Lett.* **1996**, *256*, 391.
[50] A. Siiskonen, A. Priimagi, *J. Mol. Model.* **2017**, *23*, 50.
[51] (May 2022) ed., National Institute of Standards and Technology.
[52] M. Bouilloud, N. Fray, Y. Bénilan, H. Cottin, M.-C. Gazeau, A. Jolly, *Mon. Not. R. Astron. Soc.* **2015**, *451*, 2145.
[53] D. Yerezhep, A. Akylbayeva, O. Golikov, D. Y. Sokolov, A. Shinbayeva, A. U. Aldiyarov, *ACS Omega* **2023**, *8*, 19567.
[54] A. Drobyshev, A. Aldiyarov, A. Nurmukan, D. Sokolov, A. Shinbayeva, *Low Temp. Phys.* **2018**, *44*, 831.
[55] W. Wang, Y. Zhang, B. Ji, *J. Phys. Chem. A* **2010**, *114*, 7257.
[56] X. Li, L. Liu, H. B. Schlegel, *J. Am. Chem. Soc.* **2002**, *124*, 9639.
[57] R. L. Hudson, P. A. Gerakines, Y. Y. Yarnall, *Astrophys. J.* **2024**, *970*, 108.
[58] J. He, S. J. Diamant, S. Wang, H. Yu, W. R. Rocha, M. Rachid, H. Linnartz, *Astrophys. J.* **2022**, *925*, 179.
[59] M. Brunelli, A. Fitch, *Z. Kristall.-Crystall. Mater.* **2002**, *217*, 395.

Manuscript received: September 18, 2025
Revised manuscript received: November 26, 2025
Version of record online: